1-1-2012

Synthesis of uniform TiO2@carbon composite nanofibers as anode for lithium ion batteries with enhanced electrochemical performance

Zunxian Yang
Fuzhou University

Guodong Du
University of Wollongong, gd616@uow.edu.au

Qing Meng
University of Wollongong, qm982@uowmail.edu.au

Zaiping Guo
University of Wollongong, zguo@uow.edu.au

Xuebin Yu
Fudan University, xyu@uow.edu.au

See next page for additional authors

Journal of Materials Chemistry

Cite this: J. Mater. Chem., 2012, 22, 5848

www.rsc.org/materials

PAPER

Synthesis of uniform TiO_2@carbon composite nanofibers as anode for lithium ion batteries with enhanced electrochemical performance†

Zunxian Yang,*[a] Guodong Du,[b] Qing Meng,[c] Zaiping Guo,*[bc] Xuebin Yu,*[d] Zhixin Chen,[c] Tailiang Guo[a] and Rong Zeng[b]

Received 28th September 2011, Accepted 9th January 2012
DOI: 10.1039/c2jm14852h

Very large area, uniform TiO_2@carbon composite nanofibers were easily prepared by thermal pyrolysis and oxidization of electrospun titanium(IV) isopropoxide/polyacrylonitrile (PAN) nanofibers in argon. The composite nanostructures exhibit the unique feature of having TiO_2 nanocrystals encapsulated inside a porous carbon matrix. The unique orderly-bonded nanostructure, porous characteristics, and highly conductive carbon matrix favour excellent electrochemical performance of the TiO_2@carbon nanofiber electrode. The TiO_2@carbon hybrid nanofibers exhibited highly reversible capacity of 206 mAh g^{-1} up to 100 cycles at current density of 30 mA g^{-1} and excellent cycling stability, indicating that the composite is a promising anode candidate for Li-ion batteries.

Introduction

Titanium oxide, as one of the most studied semiconducting metal oxides, has attracted special attention due to its wide potential application in many fields, such as photocatalysis,[1–7] sensors,[8,9] solar cells,[10–13] lithium-ion batteries,[14–17] *etc.* Nevertheless, especially in lithium-ion battery (LIB) applications, of the four common polymorphs of TiO_2: rutile, anatase, brookite, and TiO_2(B),[18] anatase TiO_2 has been investigated longest as a prospective electrode material because of its special crystal structure with a tetragonal body-centered space group $I4_1/1md$, and the TiO_6 octahedra sharing two adjacent edges with two other octahedra.[19,20] This special three-dimensional (3D) architecture contains many open channels which facilitate the insertion/extraction of Li^+ during discharge/charge.

Recently, a variety of one-dimensional (1D) TiO_2 nanomaterials, such as nanotubes,[16,18] nanowires,[21,22] and nanorods,[23] have been prepared and used as electrode materials in lithium ion batteries because of the shorter path for Li^+ transport and the higher surface area, which result in more side reactions with the electrolyte[15] than for bulk TiO_2. However, there are still some obstacles to their practical application in lithium ion batteries, mainly owing to the low lithium ion and electronic conductivity of 1D TiO_2 nanomaterials ($\sim 10^{-12}$ S cm^{-1}).[24] Therefore, various strategies to improve the lithium ion and electronic conductivity of TiO_2 nanomaterials, such as decoration with high conductivity materials, *e.g.*, Ag nanoparticles,[18] or dispersion of such nanoparticles into the carbon matrix,[24,25] have been reported. Furthermore, a way to improve the electrochemical lithium storage properties of 1D TiO_2 nanomaterials has been suggested, which is to enhance the porosity and surface area by forming mesopores or nanocavities,[26] and is possible due to the much shorter paths for Li^+ transport and larger interior surface area. Until now, there have been many challenges to synthesize 1D TiO_2 nanomaterials with mesopores or nanocavities.

Electrospinning is a simple method of forming continuous 1D nanofibers under electrostatic force of the charges on the surface of a liquid droplet in a sufficiently high electric field, which is applied between the capillary nozzle and the metal collector.[27,28] Herein, a relatively simple and low-cost approach to prepare TiO_2@carbon composite nanofibers by a combination of electrospinning and subsequent thermal treatments is presented. As well as combining the advantages of TiO_2 nanoparticles and carbon matrices, these TiO_2@carbon nanofibers have the unique advantages of porosity, one-dimensional nanostructure, and large surface-to-volume ratio. The TiO_2@carbon nanofibers have been investigated in a preliminary way for their potential use as an anode material for lithium ion batteries and for this application have exhibited excellent cycling stability and rate capability.

[a]*National & Local United Engineering Laboratory of Flat Panel Display Technology, Fuzhou University, Fuzhou, 350002, P. R. China. E-mail: yangzunxian@hotmail.com; Fax: +61 2 4221 5731; Tel: +61 2 4221 5225*
[b]*Institute for Superconducting & Electronic Materials, University of Wollongong, NSW 2522, Australia. E-mail: zguo@uow.edu.au; Fax: +61 2 4221 5731; Tel: +61 2 4221 5225*
[c]*School of Mechanical, Materials & Mechatronics Engineering, University of Wollongong, NSW 2522, Australia. E-mail: zguo@uow.edu.au; Fax: +61 2 4221 5731; Tel: +61 2 4221 5225*
[d]*Department of Materials Science, Fudan University, Shanghai, 200433, P. R. China. E-mail: yuxuebin@fudan.edu.cn; Fax: +61 2 4221 5731; Tel: +61 2 4221 5225*

† Electronic supplementary information (ESI) available. See DOI: 10.1039/c2jm14852h

Experimental

Synthesis of TiO_2@carbon composite nanofibers

The procedures for preparing the electrospinning solution are similar to those described previously.[29–31] Simply, 0.7 g polyacrylonitrile (PAN, MW = 150000, Aldrich) was dissolved in 5.3 g N,N-dimethylformamide (DMF, 99.8%, Aldrich) at 80 °C with vigorous stirring for 2 h (solution **No. 1**). Then, 1.20 g titanium(IV) isopropoxide (97%, Aldrich) was mixed with 2.8 g anhydrous ethanol (solution **No. 2**). Afterwards, the **No. 2** solution was added dropwise to the **No. 1** solution at 80 °C with vigorous stirring. The mixed solution was then stirred at room temperature for 3 h. The polymer solution was transferred into a 10 ml syringe with a capillary tip (0.8 mm diameter). For spinning, the set-up was similar to that described previously.[6,27,29–33] Typically, the collector was placed 9.5 cm from the spinneret to collect the nanofibers. A high voltage of 13.3 kV was applied between the spinneret and the collector by a direct-current power supply (DW-P303-5ACCD, Tianjin Dongwen High Voltage Power Supply Co., China.). The solution was pushed out of the spinneret by a syringe pump (TS2-60, Baoding Lange Constant Flux Pump Co., China) at the rate of 0.3 ml h^{-1}. The collector was kept at 180 °C during electrospinning to evaporate the solvent. After spinning for more than 20 h, the nanofiber films were easily peeled off. The electrospun nanofibers were slowly decarbonized at 500 °C for 2 h in an air environment (heating rate: <1 °C min^{-1}), or carbonized at 500 °C for 2 h in argon atmosphere (heating rate: <1 °C min^{-1}), respectively. Finally, both a white film (TiO_2 nanofibers) and a black film (TiO_2@carbon nanofibers) were obtained.

Materials characterization

Thermogravimetric analysis (TGA) and differential scanning calorimetry (DSC) of the PAN and the samples were carried out with a TGA/DSC1 type instrument (Mettler Toledo, Switzerland) at a heating rate of 10 °C min^{-1} from 25 to 1000 °C in air. The morphology was evaluated using a JEOL 7500FA field emission scanning electron microscope (FE-SEM, JEOL, Tokyo, Japan). Transmission electron microscope (TEM) investigations were performed using a JEOL 2011F analytical electron microscope (JEOL, Tokyo, Japan) operating at 200 kV. The crystal structures of the TiO_2 nanofibers and TiO_2@carbon nanofibers were investigated by X-ray diffraction (XRD) phase qualitative analysis (MMA, GBC, Australia) with Cu-Kα radiation at 40 kV and 25 mA and 2θ range from 5° to 90° (0.02° resolution). The composition of the fibers was characterized using TGA and EDX analysis. Energy dispersive X-ray spectroscopy (EDX) analysis was carried out on the JEOL 7500FA analytical electron microscope as well. X-ray photoelectron spectroscopy (XPS) experiments were carried out on a VG Scientific ESCALAB 220IXL instrument using aluminum Kα X-ray radiation during XPS analysis.

Electrochemical characterization

Electrochemical properties were measured on electrodes prepared by compressing a mixture of as-prepared TiO_2@carbon hybrid nanofibers or TiO_2 nanofibers, carbon black (Super P, MMM, Belgium), and poly(vinyl difluoride) (PVDF) binder in a weight ratio of 70 : 15 : 15, mixing with suitable amount of N-methyl-2-pyrrolidone (NMP), and pasting the slurry on copper foil. Pure lithium metal foil was used as the counter and reference electrode. The electrolyte was $LiPF_6$ (1 M) in a mixture of ethylene carbonate (EC) and dimethyl carbonate (DMC) (1 : 1 v/v; Merck KgaA, Germany). Coin cells were assembled in a high-purity argon-filled glove box (Mbraun, Unilab, Germany). The galvanostatic method was used to measure the electrochemical capacity of the electrodes at room temperature with a LAND-CT2001A instrument and a charge-discharge current density of 30 mA g^{-1}. Additionally, the rate capability of electrode was investigated using a LAND-CT2001A instrument at different charge-discharge current densities of 25 mA g^{-1}, 125 mA g^{-1}, 250 mA g^{-1}, 500 mA g^{-1}, 1250 mA g^{-1}, respectively. The cut-off potentials of the TiO_2@carbon hybrid nanofiber electrode for charge and discharge were set at 3.0 and 1.0 V *versus* Li^+/Li, respectively. Cyclic voltammetry (CV) was performed on a ChI660B electrochemical workstation.

Results and discussion

Fig. 1 shows the X-ray diffraction patterns of the as-prepared TiO_2 nanofibers and TiO_2@carbon nanofibers. As shown in Fig. 1, the X-ray diffraction (XRD) patterns of both samples reveal that the TiO_2 both in the pure TiO_2 nanofibers and in the TiO_2@carbon hybrid nanofibers is anatase TiO_2 with a tetragonal structure (JCPDS 73-1764), although much sharper peaks appear in the TiO_2 nanofiber sample (Fig. 1(a)) than in the TiO_2@carbon nanofiber sample (Fig. 1(b)), which is possibly owing to the relatively smaller crystal size in the composite and the interference of the high carbon content in the TiO_2@carbon nanofibers according to the TGA results (Fig. S1(a)†). The anatase TiO_2 belongs to space group $I4_1/amd$ (141) with lattice parameters $a = 3.776$ Å and $c = 9.468$ Å. The heat treatment of titanium composite/PAN nanofibers (TCPNFs) at 500 °C in air or in argon successfully realized the conversion from TCPNFs into pure polycrystalline anatase TiO_2 phase (Fig. S1(b)†, further confirmed by HRTEM image and SAED pattern below) and anatase TiO_2@carbon composite nanofibers, respectively.

Fig. 2 and Fig. S2† show field-emission scanning electron microscope (FE-SEM) images of the as-collected titanium

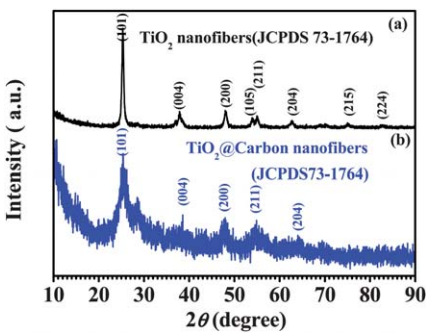

Fig. 1 X-ray diffraction patterns of as-prepared TiO_2 nanofibers and TiO_2@carbon nanofibers: (a) TiO_2 nanofibers with tetragonal structure (JCPDS 73-1764), (b) TiO_2@carbon nanofibers with same structure (JCPDS 73-1764), as indexed in the patterns.

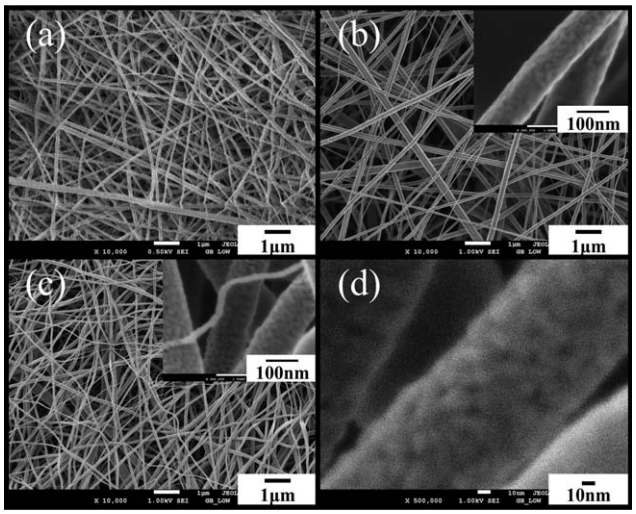

Fig. 2 FE-SEM images of as-collected titanium composite/PAN nanofibers, TiO_2@carbon nanofibers and TiO_2 nanofibers: (a) titanium composite/PAN nanofibers, (b) as-pyrolyzed TiO_2@carbon nanofibers and corresponding high magnification image (inset), (c) TiO_2 nanofibers and corresponding high magnification image (inset), (d) single TiO_2@carbon composite nanofibers with porous surface structure.

composite/PAN nanofibers, TiO_2@carbon nanofibers, and TiO_2 nanofibers. As depicted in Fig. 2(a), the FE-SEM images clearly reveal an overview of the uniform titanium composite/PAN nanofibers with diameters of 100–150 nm and lengths extending to several tens of millimetres. After calcination in argon at 500 °C for 2 h, the nanofibrous morphology is maintained (see Fig. S2(a–b)†, Fig. 2(a), Fig. 2(b), and insets), and the titanium composite/PAN nanofibers have been transformed to fully carbonized TiO_2@carbon nanofibers with diameters of 80–120 nm. These consist of orderly bonded anatase TiO_2 nanocrystals less than 10 nm in size, encapsulated in carbon matrices, which agrees well with the caculated average grain diameter (~2.3 nm) according to Debye–Scherrer formula from the (101) plane XRD of TiO_2. However, when calcined in air at 500 °C for 2 h, as shown in Fig. S2(c–d)†, Fig. 2(c–d), and insets, the as-collected titanium composite/PAN nanofibers were transformed to uniform TiO_2 nanofibers with diameters of 60–100 nm, consisting of orderly bonded pure anatase TiO_2 nanoparticles less than 15 nm in size, which is in good agreement with the caculated average grain diameter (~11.6 nm) according to Debye–Scherrer formula from the (101) plane XRD of TiO_2. Thus, to some extent, the TiO_2@carbon nanofibers can be viewed as an intermediate product in the preparation of pure TiO_2 nanofibers, but with carbon filling between the TiO_2 particles. In addition, many holes/voids were left between the bonded TiO_2@carbon or TiO_2 particles in the nanofibers, arising from the pyrolysis of PAN. Furthermore, some mesoporosities between nanofibers are shown Fig. S2†, Fig. 2(b), and Fig. 2(b–d) and insets. The holes/voids and mesoporosities formed in these nanofibers ensure a high electrode-electrolyte contact area in the hybrid nanofibers, so a large amount of lithium ions can be accommodated without any remarkable degradation of the structure during charge/discharge cycling, which is favorable to both lithium ion storage and Li^+ diffusion.

Transmission electron microscope (TEM) observations of the pyrolyzed TiO_2@carbon and pure TiO_2 nanofibers provides worthwhile structural and chemical information (Fig. 3). The high resolution TEM (HRTEM) images (Fig. 3(a)) clarify the crystal structure, as interplanar with spacing of approximately 0.36 nm between neighboring (101) planes of tetragonal TiO_2, as these planes were parallel to the electron beam. Only a few crystals have revealed clear lattice fringes in HRTEM, while other areas without lattice fringes are present. These areas could be carbon-filled regions or crystals whose orientation are not parallel to the electron beam. The crystal size of TiO_2 in these nanofibers is about 5–10 nm. Fig. 3(b) and Fig. S3(a)† demonstrate that TiO_2@carbon nanofibers are composed of many nanoparticles bonded together to form a fibrous morphology, this is further confirmed by the corresponding selected area electronic diffraction (SAED) pattern (Fig. 3(b) inset) which reveals the fine microstructure of the TiO_2@carbon nanofibers. The ring-shaped SAED pattern indicates that TiO_2 encapsulated in the TiO_2@carbon nanofibers is in polycrystalline form, similar to that reported previously.[34] The obviously spotted diffraction rings from inside to outside can be indexed to the (101), (004), and (200) planes of anatase TiO_2, respectively (Fig. 3(b) inset). When calcined in air, the pure TiO_2 nanofiber sample in Fig. 3(c) displays the same crystal structure with the same interplanar spacing of approximately 0.36 nm between neighboring (101) planes of tetragonal TiO_2, but with a crystal size of ~10–15 nm, slightly larger than the TiO_2@carbon hybrid nanofibers, possibly due to carbon interference with the growth of TiO_2 crystals in the hybrid nanofibers. Fig. 3(d) and Fig. S3(b)†display a similar polycrystalline form of these TiO_2 nanofibers, which is further confirmed by the corresponding selected-area electronic diffraction (SAED) pattern (Fig. 3(d) inset), but only in that there are more obvious spotted diffraction rings. The rings from inside to outside can be indexed to the (101), (004), (200), and (105) planes of anatase TiO_2, respectively, which is in good agreement with the XRD results described above. The TiO_2@carbon nanofibers

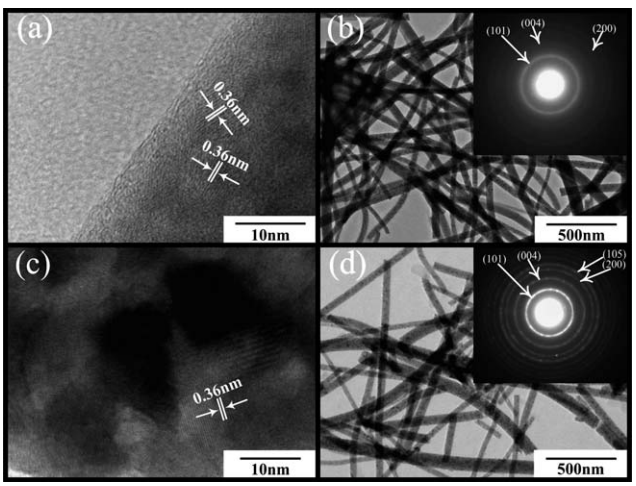

Fig. 3 (a) HRTEM image of a section of a TiO_2@carbon composite nanofiber, (b) low-magnification TEM image and SAED pattern (inset) of TiO_2@carbon composite nanofibers, (c) HRTEM image of a section of a TiO_2 nanofiber, (d) low-magnification TEM image and SAED pattern (inset) of TiO_2 nanofibers.

include mainly the elements Ti, O, and C (Fig. S3(c)†), while the pure TiO_2 nanofibers are composed of the elements Ti and O (Fig. S3(d)†). The carbon content in the TiO_2@carbon nanofibers is 34.48% according to the EDX spectra (Fig. S3(c)†), agreeing well with the TGA results (Fig. S1†).

X-ray photoelectron spectroscopy (XPS) analysis of the TiO_2@carbon and pure TiO_2 nanofibers was conducted from 0 to 1100 eV. Obvious C1s, O1s, and Ti2p peaks were detected, and their high-resolution spectra are shown in Fig. 4(a–e), respectively. The Ti2p spectrum (Fig. 4(a)) for the TiO_2@carbon hybrid nanofibers comprises two symmetrical peaks with binding energies (BEs) of 458.90 eV and 464.65 eV, which are attributable to Ti2p3/2 and Ti2p1/2, respectively, and are slightly larger than those of the pure TiO_2 nanofiber sample (Fig. 4(b)). The separation between these two peaks is 5.75 eV, slightly larger than the energy splitting reported for TiO_2[35,36] and that of the pure TiO_2 nanofibers. The cause is possibly that encapsulation of the TiO_2 in the carbon matrix influences the BEs of Ti2p electrons. As shown in Fig. 4(c), the main portion of the response could come from TiO_2, as evidenced by the O1s binding energy (BE) peak at ~530.29 eV (Fig. 4(c)) and 529.91 eV(Fig. 4(d)),[37] while the peak at 531.61 eV (Fig. 4(c)) and 531.26 eV (Fig. 4(d)) may be due to the OH^- radical, adsorbed oxygen, or carbonyl.[35,38] As for the high BE peak at 532.89 eV (Fig. 4(c)) and 532.23 eV (Fig. 4(d)), it possibly originates from absorbed H_2O. Similarly, encapsulation of TiO_2 in the carbon matrix possibly leads to the three fitted O1s peaks that are slightly larger for the TiO_2@carbon nanofibers than for the pure TiO_2 nanofibers. According to Fig. 4(e), the high resolution spectrum of the C1s region of as-prepared TiO_2@carbon hybrid nanofibers can be fitted to four peaks,

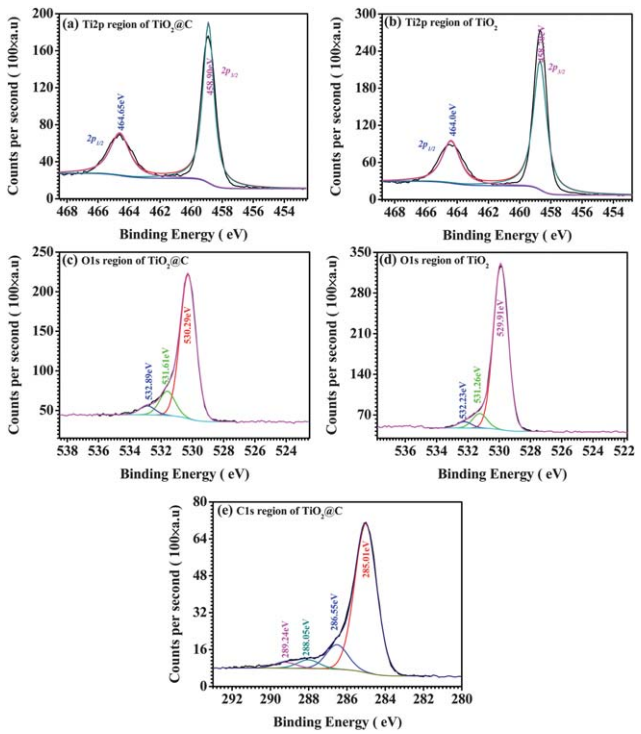

Fig. 4 XPS high-resolution spectra of the C1s, O1s, and Ti2p regions of the as-prepared TiO_2@carbon nanofibers and TiO_2 nanofibers, respectively.

including the large peak at 285.01 eV attributed to un-oxidized graphitic carbon.[38] The peak at 286.55 eV is attributed to disordered carbon or oxidant carbon, such as carbon in alcohols,[35,38] which is in good accordance with the fitted O1s peaks. The remaining two small peaks at 288.05 eV and 289.24 eV possibly come from a trace amount of carboxyl in the hybrid sample.[38] From a combination of the XRD, FE-SEM, TEM, and XPS results, it is concluded that TiO_2 in these nanofibers exists in the form of polycrystalline TiO_2. Each TiO_2 particle is possibly one small crystal because of the low diffusion capability of TiO_2 in the nanofibers at the pyrolysis temperature. In addition, many hole/void nanopores are formed between the bound TiO_2 or TiO_2@carbon particles in the nanofibers. This one-dimensional TiO_2@carbon material would introduce unique advantages in lithium ion battery application,[39] such as high conductivity due to encapsulation of the TiO_2 nanocrystals in the high carbon content, improved Li^+ and electrolyte transport in the nanofibers from the hole/void nanopores that exist between the bound TiO_2@carbon particles in the nanofibers, and so on, all of which favor the enhancement of the electrochemical performance of the electrode as compared with pure TiO_2.

The electrochemical performance of TiO_2@carbon nanofibers in the lithium ion battery has been characterized by galvanostatic discharge-charge cycling and cyclic voltammetry, as shown in Fig. 5. Cyclic voltammograms (CV) of TiO_2@carbon hybrid nanofibers from the first to the fifth cycle at a scan rate of 0.1 mV s^{-1} in the voltage range of 0.01–3.0 V were obtained and are presented in Fig. 5(a). The curves of the initial five cycles are different from the later ones, especially with respect to the subsequent gradual disappearance of some high voltage CV peaks, possibly owing to the gradual formation of an inactive solid/electrolyte interphase (SEI) on the surface of the active material, which is inclined to intercept reversible Li ion pathways in the discharge/charge processes. In the first cycle, the cathodic/anodic peak pair at 0.012 V and 0.124 V is attributed to lithium ion insertion into and extraction out of the carbon material, while another cathodic/anodic peak pair at around 0.69 V and 1.3 V suggest the decomposition of solvent, with decomposition products acting as a SEI on the surface of the active materials.[40] There remain two obvious cathodic/anodic peak pairs at 1.40 V and 1.89 V, and 1.61 V and 2.06 V in the first cycle, although the two cathodic peaks merge and stabilize at 1.50 V and 1.89 V in subsequent cycles, which are probably attributable to lithium ion insertion into/extraction out of anatase TiO_2. However, there is one unknown peak at 2.37 V in the first cycle. This peak at 2.37 V disappears in the next few cycles, and the corresponding reaction of this peak is still not clear. Further experiments such as *in situ* or *ex situ* synchrotron or Raman analysis, need to be conducted in order to understand this in future.

Galvanostatic discharge/charge experiments on the TiO_2@carbon nanofiber electrodes were carried out in the voltage range of 3.0–1.0 V (*versus* Li/Li^+) at a constant current density of approximately 30 mA g^{-1} up to 100 cycles. Fig. 5(b) presents the voltage profiles of a TiO_2@carbon hybrid nanofiber electrode at the current density of 30 mA g^{-1}. The first discharge and charge steps deliver a specific capacity of 220.8 and 217.1 mAh g^{-1}, respectively, much higher than for pure TiO_2 nanofiber electrode, *i.e.* 182.7 and 178.5 mAh g^{-1} (Fig. 5(c)). The initial coulombic efficiency of the TiO_2@carbon nanofibers electrode is above

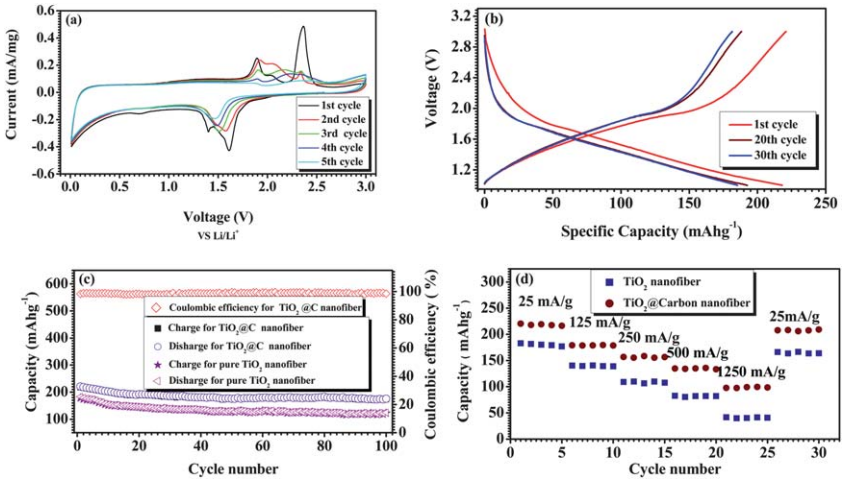

Fig. 5 Electrochemical performance of TiO_2@carbon nanofiber and TiO_2 nanofiber electrodes cycled between 1.0 and 3.0 V *vs.* Li^+/Li: (a) Cyclic voltammograms of TiO_2@carbon nanofiber electrode from the first cycle to the fifth cycle at a scan rate of 0.1 mV s^{-1} in the voltage range of 0.0–3.0 V. (b) Voltage profiles for selected cycles of TiO_2@carbon nanofiber composite electrode at the current density of 30 mA g^{-1}. (c) Capacity *vs.* cycle number curves and coulombic efficiency from the first cycle to the 100th cycle for the TiO_2@carbon nanofibers and pure TiO_2 nanofibers at the current density of 30 mA g^{-1}. (d) Rate capabilities of TiO_2 and TiO_2@carbon electrodes at various currents.

98.324%, slightly higher than that of the pure TiO_2 nanofiber electrode (97.6%) and those of some reported pure TiO_2 nanotube electrodes.[16] Fig. 5(c) shows the curves of discharge capacity *versus* cycle number for the TiO_2@carbon nanofiber and pure TiO_2 nanofiber electrodes at current density 30 mA g^{-1}. The TiO_2@carbon composite electrode exhibits excellent cyclic performance and a high reversible specific capacity of over 200 mAh g^{-1} in the first 50 cycles, and it maintains a reversible capacity after 100 cycles of approximately 206 mAh g^{-1} with high coulombic efficiency of nearly 100%, much higher than the specific capacity and coulombic efficiency of the pure TiO_2 nanofiber electrode and those reported pure TiO_2 nanotube electrode[16] and TiO_2–carbon composite nanotube electrodes.[24] An additional advantage of the TiO_2@carbon hybrid nanofiber electrode is the enhancement of rate capability due to the short Li^+ diffusion paths and easy access of the electrolyte through interconnected pores, as well as the good electrical connectivity. The rate capability testing results are shown in Fig. 5 (d). Compared with the bare TiO_2 porous nanofiber electrode, the TiO_2@carbon hybrid nanofiber electrode exhibits excellent rate performance; it delivers discharge capacity of over 220 mAh g^{-1} at current density of 25 mA g^{-1}, 179.17 mAh g^{-1} at 125 mA g^{-1}, 156.83 mAh g^{-1} at 250 mA g^{-1}, 134.55 mAh g^{-1} at 500 mA g^{-1}, finally around 100 mAh g^{-1} at current density of 1250 mA g^{-1}, respectively, which is better than those of reported pure TiO_2 nanotube[16] and TiO_2–carbon nanotube electordes.[24,25] The improved initial capacity, coulombic efficiency, reversible discharge capacity, and rate capability of the TiO_2@carbon nanofiber electrode were attributed to the small crystal size of the TiO_2 and the porous nature of the TiO_2@carbon nanofibers (Fig. 2 and Fig. 3), as well as the high conductivity owing to the high carbon content in the composite (Fig. S3†).

As demonstrated in Scheme S1†, TiO_2@carbon nanoparticles, consisting of TiO_2 nanocrystals inside porous hard carbon, bond together in a nanofiber to form TiO_2@carbon hybrid nanofiber, which possesses many hole/void nanopores due to pyrolysis of PAN during the heat treatment process. Although there are also many nanopores between the TiO_2 nanofibers, which are also composed of TiO_2 nanoparticles bonded together in a nanofiber form, the relatively poor electrochemical performance of the TiO_2 nanofiber electrode should possibly be ascribed to its relatively lower conductivity. Accordingly, the porous TiO_2@carbon nanofibers with relatively higher specific surface area compared to micron-sized particles ensure good electrode-electrolyte contact and short lithium ion diffusion pathways during discharge/charge cycling, and thus make a great contribution to lithium storage capacity. Additionally, the carbon matrix in the composite enhances the conductivity of the active materials during lithium intercalation/de-intercalation, which plays a critical role in the excellent lithium storage capacity and cyclability of the electrode.

Conclusions

In summary, under optimized synthesis conditions including the composition and concentration of electrospun solution and electrospun parameters such as temperature of collector, the distance between collector and spinet, pushing velocity of solution and applied voltage between spinet and collector and so on, very large area (4 cm × 2.5 cm), uniform TiO_2@carbon and TiO_2 nanofibers consisting of orderly bonded nanoparticles were prepared by thermal pyrolysis and oxidization of titanium(IV) isopropoxide/polyacrylonitrile (PAN) nanofibers in argon *via* a simple electrospinning technology for the first time. As a potential anode material for lithium ion batteries, these TiO_2@carbon hybrid nanofibers display a high initial reversible capacity of 217.1 mAh g^{-1} with high coulombic efficiency of nearly 100% at the current density of 30 mA g^{-1} and deliver a high reversible specific capacity of over 200 mAh g^{-1} in the first 50 cycles, and further maintain a reversible capacity after 100 cycles of approximately 206 mAh g^{-1} with high coulombic efficiency of nearly 100%, much higher than that of the pure TiO_2 nanofiber electrode. This particular orderly-bonded nanoparticle composite architecture is characterized by many nanopores in

the nanofibers. These nanopores facilitate lithium ion and electrolyte diffusion in the active materials during charge/discharge processes. Furthermore, the high carbon content matrix in the TiO_2@carbon hybrid nanofibers acts to encapsulate the TiO_2 nanocrystals and enhance the conductivity of the active material, as compared with pure TiO_2 nanofibers. Therefore, the composite is a very promising potential anode material for LIBs, even though the composition and structure of these materials require further improvement.

Acknowledgements

Part of the work was funded by the Australian Research Council (ARC) through a Discovery project (DP1094261), the Post-doctoral Foundation Program of Fuzhou University (BSH-0601), the Natural Science Foundation Program of Fujian Province (2010J01332, A0510011), the Foundation Program of the Ministry of Education for Returned Exchange Personnel (LXKQ201101), and the Talent Foundation Program of Fuzhou University. The authors also would like to thank Dr Tania Silver at the University of Wollongong for critical reading of the manuscript and Mr. Darren Attard for his contribution.

References

1 Yang Bai, Wei Li, Chang Liu, Zhuhong Yang, Xin Feng, Xiaohua Lu and Kwong-Yu Chan, Stability of Pt nanoparticles and enhanced photocatalytic performance in mesoporous Pt-(anatase/TiO2(B)) nanoarchitecture, *J. Mater. Chem.*, 2009, **19**(38), 7055.
2 M. R. S. Castro, E. D. Sam, M. Veith and P. W. Oliveira, Structure, wettability and photocatalytic activity of CO2 laser sintered TiO2/multi-walled carbon nanotube coatings, *Nanotechnology*, 2008, **19**(10), 105704.
3 X. Y. Chen, S. X. Liu and X. Q. Zhang, Preparation and properties of activated carbon supported nitrogen doped visible-light response TiO2-xNy/AC photocatalysts, *J. Inorg. Mater.*, 2008, **23**(3), 464–470.
4 K. H. Ji, D. M. Jang, Y. J. Cho, Y. Myung, H. S. Kim, Y. Kim and J. Park, Comparative Photocatalytic Ability of Nanocrystal-Carbon Nanotube and -TiO2 Nanocrystal Hybrid Nanostructures, *J. Phys. Chem. C*, 2009, **113**(46), 19966–19972.
5 C. H. Lin, J. H. Chao, C. H. Liu, J. C. Chang and F. C. Wang, Effect of calcination temperature on the structure of a Pt/TiO2 (B) nanofiber and its photocatalytic activity in generating H-2, *Langmuir*, 2008, **24**(17), 9907–9915.
6 Zhaoyang Liu, Darren Delai Sun, Peng Guo and James O. Leckie, An Efficient Bicomponent TiO2/SnO2Nanofiber Photocatalyst Fabricated by Electrospinning with a Side-by-Side Dual Spinneret Method, *Nano Lett.*, 2007, **7**(4), 1081–1085.
7 Karran Woan, Georgios Pyrgiotakis and Wolfgang Sigmund, Photocatalytic Carbon-Nanotube-TiO2Composites, *Adv. Mater.*, 2009, **21**(21), 2233–2239.
8 G. Wang, Q. Wang, W. Lu and J. H. Li, Photoelectrochemical study on charge transfer properties of TiO2-B nanowires with an application as humidity sensors, *J. Phys. Chem. B*, 2006, **110**(43), 22029–22034.
9 Hongnan Zhang, Zhenyu Li, Li Liu, Ce Wang, Yen Wei and Alan G. MacDiarmid, Mg2+/Na+-doped rutile TiO2 nanofiber mats for high-speed and anti-fogged humidity sensors, *Talanta*, 2009, **79**(3), 953–958.
10 Jing-Hong Huang, Po Yu Hung, Shu-Fen Hu and Ru-Shi Liu, Improvement efficiency of a dye-sensitized solar cell using Eu3+ modified TiO2 nanoparticles as a secondary layer electrode, *J. Mater. Chem.*, 2010, **20**(31), 6505.
11 Kai Pan, Youzhen Dong, Chungui Tian, Wei Zhou, Guohui Tian, Baofeng Zhao and Honggang Fu, TiO2-B narrow nanobelt/TiO2 nanoparticle composite photoelectrode for dye-sensitized solar cells, *Electrochim. Acta*, 2009, **54**(28), 7350–7356.
12 C. Rochford, Z. Z. Li, J. Baca, J. W. Liu, J. Li and J. Wu, The effect of annealing on the photoconductivity of carbon nanofiber/TiO2 core-shell nanowires for use in dye-sensitized solar cells, *Appl. Phys. Lett.*, 2010, 97.
13 Xia Wu, Gao Qing Lu and Lianzhou Wang, Shell-in-shell TiO2 hollow spheres synthesized by one-pot hydrothermal method for dye-sensitized solar cell application, *Energy Environ. Sci.*, 2011, **4**(9), 3565–3572.
14 M. Wagemaker, A. P. M. Kentgens and F. M. Mulder, Equilibrium lithium transport between nanocrystalline phases in intercalated TiO2 anatase, *Nature*, 2002, **418**(6896), 397–399.
15 Da Deng, Min Gyu Kim, Jim Yang Lee and Jaephil Cho, Green energy storage materials: Nanostructured TiO2 and Sn-based anodes for lithium-ion batteries, *Energy Environ. Sci.*, 2009, **2**(8), 818.
16 J. Xu, C. Jia, B. Cao and W. Zhang, Electrochemical properties of anatase TiO2 nanotubes as an anode material for lithium-ion batteries, *Electrochim. Acta*, 2007, **52**(28), 8044–8047.
17 G. Armstrong, A. R. Armstrong, P. G. Bruce, P. Reale and B. Scrosati, TiO2(B) Nanowires as an Improved Anode Material for Lithium-Ion Batteries Containing LiFePO4 or LiNi0.5Mn1.5O4 Cathodes and a Polymer Electrolyte, *Adv. Mater.*, 2006, **18**(19), 2597–2600.
18 B. He, B. Dong and H. Li, Preparation and electrochemical properties of Ag-modified TiO2 nanotube anode material for lithium–ion battery, *Electrochem. Commun.*, 2007, **9**(3), 425–430.
19 Jinyoung Kim and Jaephil Cho, Rate Characteristics of Anatase TiO [sub 2] Nanotubes and Nanorods for Lithium Battery Anode Materials at Room Temperature, *J. Electrochem. Soc.*, 2007, **154**(6), A542.
20 J. S. Chen, Y. L. Tan, C. M. Li, Y. L. Cheah, D. Y. Luan, S. Madhavi, F. Y. C. Boey, L. A. Archer and X. W. Lou, Constructing Hierarchical Spheres from Large Ultrathin Anatase TiO2 Nanosheets with Nearly 100% Exposed (001) Facets for Fast Reversible Lithium Storage, *J. Am. Chem. Soc.*, 2010, **132**(17), 6124–6130.
21 Y. Wang, M. Wu and W. Zhang, Preparation and electrochemical characterization of TiO2 nanowires as an electrode material for lithium-ion batteries, *Electrochim. Acta*, 2008, **53**(27), 7863–7868.
22 A. R. Armstrong, G. Armstrong, J. Canales, R. Garcia and P. G. Bruce, Lithium-ion intercalation into TiO2-B nanowires, *Adv. Mater.*, 2005, **17**(7), 862.
23 H. Qiao, Y. Wang, L. Xiao and L. Zhang, High lithium electroactivity of hierarchical porous rutile TiO2 nanorod microspheres, *Electrochem. Commun.*, 2008, **10**(9), 1280–1283.
24 S. Yoon, B. H. Ka, C. Lee, M. Park and S. M. Oh, Preparation of Nanotube TiO2-Carbon Composite and Its Anode Performance in Lithium-Ion Batteries, *Electrochem. Solid-State Lett.*, 2009, **12**(2), A28–A32.
25 J. Xu, Y. Wang, Z. Li and W. Zhang, Preparation and electrochemical properties of carbon-doped TiO2 nanotubes as an anode material for lithium-ion batteries, *J. Power Sources*, 2008, **175**(2), 903–908.
26 Q. J. Li, J. W. Zhang, B. B. Liu, M. Li, R. Liu, X. L. Li, H. L. Ma, S. D. Yu, L. Wang, Y. G. Zou, Z. P. Li, B. Zou, T. Cui and G. T. Zou, Synthesis of High-Density Nanocavities inside TiO2-B Nanoribbons and Their Enhanced Electrochemical Lithium Storage Properties, *Inorg. Chem.*, 2008, **47**(21), 9870–9873.
27 C. Kim, K. S. Yang, M. Kojima, K. Yoshida, Y. J. Kim, Y. A. Kim and M. Endo, Fabrication of Electrospinning-Derived Carbon Nanofiber Webs for the Anode Material of Lithium-Ion Secondary Batteries, *Adv. Funct. Mater.*, 2006, **16**(18), 2393–2397.
28 D. Li and Y. N. Xia, Electrospinning of nanofibers: Reinventing the wheel?, *Adv. Mater.*, 2004, **16**(14), 1151–1170.
29 Z. X. Yang, G. D. Du, C. Q. Feng, S. A. Li, Z. X. Chen, P. Zhang, Z. P. Guo, X. B. Yu, G. N. Chen, S. Z. Huang and H. K. Liu, Synthesis of uniform polycrystalline tin dioxide nanofibers and electrochemical application in lithium-ion batteries, *Electrochim. Acta*, 2010, **55**(19), 5485–5491.
30 Z. X. Yang, G. D. Du, Z. P. Guo, X. B. Yu, Z. X. Chen, P. Zhang, G. N. Chen and H. K. Liu, Easy preparation of SnO2@carbon composite nanofibers with improved lithium ion storage properties, *J. Mater. Res.*, 2010, **25**(8), 1516–1524.
31 Z. X. Yang, G. D. Du, Z. P. Guo, X. B. Yu, S. A. Li, Z. X. Chen, P. Zhang and H. K. Liu, Plum-branch-like carbon nanofibers decorated with SnO2 nanocrystals, *Nanoscale*, 2010, **2**(6), 1011–1017.

32 H. Wang, Y. Wang, Y. Yang, X. Li and C. Wang, Photoluminescence properties of the rare-earth ions in the TiO2 host nanofibers prepared *via* electrospinning, *Mater. Res. Bull.*, 2009, **44**(2), 408–414.
33 Guoping Dong, Xiudi Xiao, Yingzhi Chi, Bin Qian, Xiaofeng Liu, Zhijun Ma, Song Ye, E. Wu, Heping Zeng, Danping Chen and Jianrong Qiu, Polarized Luminescence Properties of TiO2:Sm3 + Microfibers and Microbelts Prepared by Electrospinning, *J. Phys. Chem. C*, 2009, **113**(22), 9595–9600.
34 G. Wang, Y. Ji, X. R. Huang, X. Q. Yang, P. I. Gouma and M. Dudley, Fabrication and characterization of polycrystalline WO3 nanofibers and their application for ammonia sensing, *J. Phys. Chem. B*, 2006, **110**(47), 23777–23782.
35 Naofumi Ohtsu, Naoya Masahashi, Yoshiteru Mizukoshi and Kazuaki Wagatsuma, Hydrocarbon Decomposition on a Hydrophilic TiO2Surface by UV Irradiation: Spectral and Quantitative Analysis Using in situ XPS Technique, *Langmuir*, 2009, **25**(19), 11586–11591.
36 S. Ben Amor, G. Baud, M. Benmalek, H. Dunlop, R. Frier and M. Jacquet, Titania Coatings on Polyethylene Terephthalate: Adhesion and XPS Studies., *J. Adhes.*, 1998, **65**(1), 307–329.
37 Caixian Chang, Jiangfeng Xiang, Ming Li, Xiaoyan Han, Liangjie Yuan and Jutang Sun, Improved disordered carbon as high performance anode material for lithium ion battery, *J. Solid State Electrochem.*, 2008, **13**(3), 427–431.
38 XPS database on Web:http://www.lasurface.com/database/elementxps.php (April 2011).
39 Liwen Ji and Xiangwu Zhang, Electrospun carbon nanofibers containing silicon particles as an energy-storage medium, *Carbon*, 2009, **47**(14), 3219–3226.
40 Y. T. MatsuoFukutsuka, Y. Sugie, A. Takeshi, M. Inaba and Z. Ogumi, Surface modification of carbonaceous thin films by NF3 plasma and their effects on electrochemical properties, *Molecular Crystals and Liquid Crystals*, 2002, **388**, 531–536.

